mathematics

MDPI

Article

Gain-Switched Short Pulse Generation from 1.55 μm InAs/InP/(113)B Quantum Dot Laser Modeled Using Multi-Population Rate Equations

Hilal S. Duranoglu Tunc [1], Nuran Dogru [2,*] and Erkan Cengiz [2]

[1] Radio Frequency and Photonics Engineering, Dresden University of Technology, 01069 Dresden, Germany
[2] Electrical and Electronics Engineering, University of Gaziantep, 27310 Gaziantep, Turkey
* Correspondence: dogru@gantep.edu.tr; Tel.: +90-342-3172132

Abstract: The gain-switching properties of an InAs-InP (113)B quantum dot laser based on multi-population rate equations are examined theoretically in detail to generate shorter pulses with the application of a Gaussian pulse beam to the laser excited state. The numerical results demonstrated that as the homogeneous and the inhomogeneous broadening increase, the differential gain, the gain compression factor, and the threshold current of the excited state decrease while the threshold current of the ground state increases. It was also observed that the contribution of the excited state to gain-switched output pulses depend on not only the value of the inhomogeneous broadening but also the magnitude of the applied current. Additionally, it was found that without an optical beam, the output pulse has a long pulse width due to ground state emissions and the change in the parameters strongly affecting the output. However, under the optical beam, narrow pulses around 26 ps have high peak power owing to the excited state emission generated even at low currents and also the change in the laser parameters having a negligible effect. Finally, the gain-switching characteristics with and without a Gaussian pulse beam are shown to be similar for liner-gain and nonlinear-gain cases except that higher peak power and narrower output pulses are obtained for the linear-gain case.

Keywords: gain-switching; semiconductor laser; quantum-dot; homogeneous-broadening; inhomogeneous-broadening; pulse generation

MSC: 78M99; 65M99

Citation: Tunc, H.S.D.; Dogru, N.; Cengiz, E. Gain-Switched Short Pulse Generation from 1.55 μm InAs/InP/(113)B Quantum Dot Laser Modeled Using Multi-Population Rate Equations. *Mathematics* **2022**, *10*, 4316. https://doi.org/10.3390/math10224316

Academic Editors: Shujin Laima, Yong Cao, Xiaowei Jin and Hehe Ren

Received: 22 September 2022
Accepted: 24 October 2022
Published: 17 November 2022

1. Introduction

Quantum dot lasers have superior features compared to quantum well counterparts [1–4] such as temperature independence, a low threshold current [5], they can be operated with low chirp for both ground state (Grs) and excited state (Exs) lasing [4], and have better resistance values for optical feedback [6]. The feature of being relatively insensitive to temperature makes quantum dot (Q-Dot) lasers avoid the need for thermoelectric coolers [7]. Since these mentioned features mean that Q-Dot lasers are compact, cheap, lightweight, and low power systems, they are appropriate candidates for applications in optical communications [7].

Low-cost directly adjustable lasers will play an important role in next-generation telecommunication links for developing uncooled and non-insulating communication devices. As a result, Q-Dot lasers are very promising for such applications. In optical communication systems, a 1.55 μm light source is required because of the low loss in transmission. InGaAs-GaAs Q-Dot devices do not allow laser emissions over 1.45 μm, which causes information loss in long-distance transmissions. For this reason, to achieve standard long-distance transmission, one uses long-haul optical transmission at a wavelength of up to 1.55 μm. Consequently, one chooses the InAs-InP(113)B Q-Dot lasers with the InAs Q-Dot laser grown on an InP substrate that emits at a wavelength of 1.55 μm [3,8,9]. Owing to their

simple fabrication methods and low manufacturing costs, the gain-switched semiconductor laser diodes are preferred over their counterparts. Therefore, in this study, we used the gain-switching method to obtain short pulses. To date, although several studies have been performed to investigate 1.55 μm InAs-InP Q-Dot lasers, to the best of our knowledge, no detailed work has been performed under the gain-switching condition for InAs-InP Q-Dot lasers based on multi-population rate equations involving nonlinear gain. For this, an external optical Gaussian beam (EOGB) was applied to the excited state (Exs) of the Q-Dot laser with current injection to the wetting layer (Wly) to investigate the properties of the gain-switched pulses. Although, Q-Dot lasers have superior performance, they cannot always satisfy the expected features in reality due to the homogeneous and inhomogeneous broadenings and the gain compression factor [10–12]. To obtain an appropriate and suitable approach to experimental results theoretically, as many aspects of real experiments as possible should be taken into account when performing the simulation. For this, the effect of the homogeneous and the inhomogeneous broadening with the effect of the gain compression were taken into consideration in this study. Therefore, this paper is organized as follows: Section 2 introduces the theoretical description of multi-population rate equations for the direct relaxation model considering the nonlinear-gain case. The obtained results discussed in Section 3 show that by applying an EOGB into the Exs, very short pulses, with a pulse width of around 26 ps and high peak power, are generated due to the Exs emissions at low currents. In addition, it was shown that the contribution of excited state to gain-switched output pulses does not depend on only the value of the inhomogeneous broadening but also on the magnitude of the applied current. Furthermore, the effect of homogeneous and inhomogeneous broadening on the differential gain, the gain compression factor, and the threshold current is also investigated. Finally, our results are summarized and concluded in Section 4.

2. Materials and Methods

The laser model used in this study for InAs-InP(113)B Q-Dot is based on the multi population rate equations for the direct relaxation model described in [2,11,13]. The laser carrier and photon density equations were solved by the fourth order Runge–Kutta method using MATLAB software to investigate the carrier dynamics in the two lowest energy levels, Grs and Exs. The initial values of carrier and photon densities were taken to be a zero. A stimulated emission term was also added to the Exs to allow lasing from both states. The effect of temperature and carrier loss were neglected in the study. We assumed that the carriers were directly injected from the contacts to the Wly; therefore, the carrier dynamics were not considered in the barrier. Direct transition from the Wly to the Grs was introduced to reproduce the experimental results [2,11,13]. The Q-Dot active region consists of the Q-Dots ensemble having different sizes. In the model, in order to consider the effect of the inhomogeneous broadening (Γ_{ihom}), the Q-Dot ensemble is divided into 2X + 1 groups, depending on their resonant energies for the interband transition [14,15]. Figure 1 shows the relaxation mechanisms in the xth Q-Dot subgroup. Energies of Exs and Grs of xth Q-Dot are represented as E_{Exs_x} and E_{Grs_x}, respectively. As a result, the longitudinal cavity photon modes of up to 2P + 1 are constructed in the cavity [13]. When the index x is equal to X, this situation corresponds to the central Q-Dot group. When index p is equal to P, this case corresponds to the central mode with the transitional energies of E_{Exs0} and E_{Grs0} for Exs and Grs, respectively. Each Q-Dot group energy width (ΔE) and mode energy separation (ΔE_p) are assumed to be equal and taken to be as 1 meV [13]. The xth Q-Dot group energy and pth mode energies are indicated by:

$$E_{Exs\_x,Grs\_x} = E_{Exs0,Grs0} - (X - x)\Delta \mathrm{E} \quad x = 1, 2, \ldots, 2X + 1, \tag{1}$$

$$E_{Exs\_p\ ,\ Grs\_p} = E_{Exs0,Grs0} - (P - p)\Delta E_p \quad p = 1, 2, \ldots, 2P + 1, \tag{2}$$

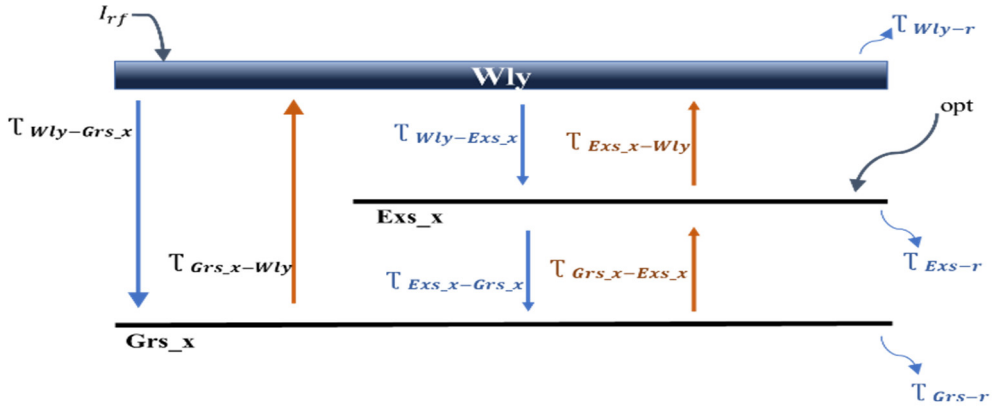

Figure 1. Schematic representation of carrier dynamics for xth QD subgroup.

When injection current I is applied to the Wly of the Q-Dot laser, some carriers move to the lower state E_{Exs-x} and E_{Grs-x} with a capture time of $\tau_{Wly-Exs\_x}$ for the transition from the Wly to E_{Exs_x} and a relaxation time of $\tau_{Wly-Grs\_x}$ for the Wly to the E_{Grs_x} transition. Some photons are emitted from the Wly due to spontaneous emission over a time τ_{Wly-r}. However, in the Exs, some carriers are relaxed into the E_{Grs_x} with a relaxation time $\tau_{\mathrm{Exs\_x-Grs\_x}}$. Furthermore, the more energetic carriers are thermally transferred to the Wly with a time $\tau_{\mathrm{Exs\_x-Wly}}$. The other carriers recombine spontaneously with an emission time $\tau_{\mathrm{Exs-r}}$ or by the stimulated emission of photons. The same mechanism for the carrier dynamics transitions is applied at the Grs level. The same processes occur for the carrier population in the Grs level with regard to the Exs.

The capture and relaxation times can be calculated [13] as:

$$\tau_{Wly-Exs\_x} = \frac{1}{(A_{Wly} + C_{Wly}N_{Wly})(1 - f_{Exs\_x})(G_{xExs})}, \tag{3}$$

$$\tau_{Exs\_x-Grs\_x} = \frac{1}{(A_{Exs} + C_{Exs}N_{Wly})(1 - f_{Grs\_x})}, \tag{4}$$

$$\tau_{Wly-Grs\_x} = \frac{1}{(A_{Wly} + C_{Wly}N_{Wly})(1 - f_{Grs\_x})(G_{xGrs})}, \tag{5}$$

Here, N_{Wly} is the carrier density in the Wly, $A_{Wly,Exs}$, $C_{Wly,Exs}$ are the phonon and Auger coefficients in the Wly and Exs, respectively. Their values are estimated experimentally [16]. $f_{Exs\_x,\ Grs\_x}$ is the occupation probabilities in xth group of Q-Dot in the Exs and Grs.

$$f_{Exs\_x} = \frac{N_{Exs\_x}}{\mu_{Exs}N_oG_{xExs}}, f_{Grs\_x} = \frac{N_{Grs\_x}}{\mu_{Grs}N_oG_{xGrs}}, \tag{6}$$

$\mu_{Exs,\ Grs}$ is the degeneracy of the Exs and Grs,
N_o is the Q-Dot density and
$N_{Exs\_x,\ Grs\_x}$ is the carrier density in the Exs and Grs of xth Q-Dot.
$G_{xExs,\ xGrs}$ is the density rate of xth Q-Dot in the Exs and Grs.

To calculate $G_{xExs,\ xGrs}$, the Q-Dot size distribution is assumed to be a Gaussian function given as:

$$G_{xExs,xGrs} = G_{inh,Exs,Grs}(E_{Exs\_x,Grs\_x} - E_{Exs0,Grs0})\Delta E, \tag{7}$$

$$G_{inh,Exs,Grs}(E_{Exs\_x,Grs\_x} - E_{Exs0,Grs0}) = \frac{1}{\sqrt{2\pi}\sigma}exp\left(-\frac{(E_{Exs\_x,Grs\_x} - E_{Exs0,Grs0})^2}{2\sigma^2}\right), \tag{8}$$

The full-width half-maximum of the Gaussian function is given as Γ_{inh} = 2.35 σ. In other words, Γ_{inh} is described as inhomogeneous broadening. The carrier escape time is related to the carrier capture time [17] and given as:

$$\tau_{Exs\_x-Wly} = \tau_{Wly-Exs\_x}\frac{\mu_{Exs}}{\mu_{Wly}}e^{(E_{Wly}-E_{Exs\_x})/k_BT}, \tag{9}$$

$$\tau_{Grs\_x-Wly} = \tau_{Wly-Grs\_x}\frac{\mu_{Grs}}{\mu_{Wly}}e^{(E_{Wly}-E_{Grs\_x})/k_BT}, \tag{10}$$

$$\tau_{Grs\_x-Exs\_x} = \tau_{Exs\_x-Grs\_x}\frac{\mu_{Grs}}{\mu_{Exs}}e^{(E_{Exs\_x}-E_{Grs\_x})/k_BT}, \tag{11}$$

where μ_{Wly} is the degeneracy of the Wly, k_B is the Boltzmann constant, T is the temperature, and E_{Wly} is the energy of the Wly.

Change in the carrier density in the Wly, Exs, and Grs and change in the photon density in the Exs and Grs for the multi-modes rate equations are given as:

$$\frac{dN_{Wly}}{dt} = \frac{I}{qV} + \sum_x \frac{N_{Exs\_x}}{\tau_{Exs\_x-Wly}} + \sum_x \frac{N_{Grs\_x}}{\tau_{Grs\_x-Wly}} - \frac{N_{Wly}}{\overline{\tau_{Wly-Exs}}} - \frac{N_{Wly}}{\overline{\tau_{Wly-Grs}}} - \frac{N_{Wly}}{\tau_{Wly-r}}, \tag{12}$$

$$\frac{dN_{Exs\_x}}{dt} = \frac{N_{Wly}}{\overline{\tau_{Wly-Exs\_x}}} + \frac{N_{Grs\_x}(1-f_{Exs\_x})}{\tau_{Grs\_x-Exs\_x}} - \frac{N_{Exs_x}}{\tau_{Exs_x-Grs_x}} - \frac{N_{Exs_x}}{\tau_{Exs_x-Wly}} - \frac{N_{Exs_x}}{\tau_{Exs-r}} - \Gamma v_g \sum_p g_{pxExs}S_{Exsp} + \Gamma v_g \frac{(1-f_{Exs_x})g_{pxExs}}{(2f_{Exs_x}-1)}opt, \tag{13}$$

$$\frac{dN_{Grs\_x}}{dt} = \frac{N_{Wly}}{\overline{\tau_{Wly-Grs}}} + \frac{N_{Exs\_x}}{\tau_{Exs\_x-Grs\_x}} - \frac{N_{Grs_x}(1-f_{Exs_x})}{\tau_{Grs_x-Exs_x}} - \frac{N_{Grs_x}}{\tau_{Grs_x-Wly}} - \frac{N_{Grs_x}}{\tau_{Grs-r}} - \Gamma v_g \sum_p g_{pxGrs}S_{Grsp}, \tag{14}$$

V is the volume, q is the charge, Γ is the confinement factor, and v_g is the group velocity. $\overline{\tau_{Wly-Exs}}$, and $\overline{\tau_{Wly-Grs}}$ indicate the average capture times from the Wly to Exs and from the Wly to Grs in Q-Dot ensemble. They are defined as follows:

$$\overline{\tau_{Wly-Exs}} = \sum_x \frac{1}{\left(A_{Wly} + C_{Wly}N_{Wly}\right)(1-f_{Exs\_x})(G_{xExs})}, \tag{15}$$

$$\overline{\tau_{Wly-Grs}} = \sum_x \frac{1}{\left(A_{Wly} + C_{Wly}N_{Wly}\right)(1-f_{Grs\_x})(G_{xGrs})}, \tag{16}$$

Nonlinear gain in Exs and Grs is given as:

$$g_{pxExs} = \mu_{Exs}\frac{\pi q^2\hbar}{cn_r\varepsilon_0 m_0^2}N_o\frac{\left|P_{Exs}^{\sigma}\right|^2}{E_{Exs\_x}}(2f_{Exs\_x}-1)G_{xExs}L_{Exs}\left(E_{Exs\_p}-E_{Exs\_x}\right)\frac{1}{1+\varepsilon_{Exsp}S_{Exsp}}, \tag{17}$$

$$g_{pxGrs} = \mu_{Grs}\frac{\pi q^2\hbar}{cn_r\varepsilon_0 m_0^2}N_o\frac{\left|P_{Grs}^{\sigma}\right|^2}{E_{Grs_x}}(2f_{Grs\_x}-1)G_{xGrs}L_{Grs}\left(E_{Grs\_p}-E_{Grs\_x}\right)\frac{1}{1+\varepsilon_{\ Grsp}S_{Grsp}}, \tag{18}$$

c, ε_o, $\hbar$, n_r, and m_o are the speed of light, dielectric constant in free space, Planck constant, refractive index of active medium, and free mass of electron, respectively. $\left|P_{Exs,\ Grs}^{\sigma}\right|^2$, is the transition matrix element [10] and it is estimated approximately at $2m_oE_{Exs0,Grs0}$ for InAs [17]. $S_{Exs\_p,\ Grs\_p}$ is the photon density of the pth mode emitted from Exs and Grs. The homogeneous broadening of the stimulated emission process is assumed to be Lorentzian such that $L_{Exs,Grs}\left(E_{Grs\_p}-E_{Grs\_x}\right)$,

$$L_{Exs,Grs}\left(E_{Exs\_p,\ Grs\_p}-E_{Exs\_x,\ Grs\_x}\right) = \frac{\Gamma_{hom}/\pi}{\left(E_{Exs\_p,\ Grs\_p}-E_{Exs\_x,\ Grs\_x}\right)^2+\left(\Gamma_{hom}\right)^2}, \tag{19}$$

Γ_{hom} is the full-width half-maximum of homogeneous broadening.

The gain saturation parameter, $\varepsilon_{Exsp,Grsp}$ of the Exs and Grs, is given as:

$$\varepsilon_{Exsp,\,Grsp} = \frac{hq^2\tau_p \left|P^{\partial}_{Exs,\,Grs}\right|^2}{2n_r^2\epsilon_0 m_0^2\, E_{Exs\_p,\,Grs\_p}} L_{Exs,\,Grs}\left(E_{Exs\_p,\,Grs\_p} - E_{Exs0,\,Grs0}\right), \quad (20)$$

where τ_p is the photon lifetime and it is computed from the following equations:

$$\frac{1}{\tau_p} = v_g[\alpha_{int} + \frac{1}{2L}\ln(\frac{1}{R1R2})], \quad (21)$$

where R1 and R2 are the reflectivities of the mirrors and L is the length of the laser. α_{int} is the internal loss, while the mirror loss is calculated using to the equation: $\ln(1/R1R2)/(2Ln_r)$.

$L_{Exs,Grs}\left(E_{Exs\_p,Grs\_p} - E_{Exs0,Grs0}\right)$ in Equation (20) is the Lorentzian function and given as:

$$L_{Exs,Grs}\left(E_{Exs\_p,\,Grs\_p} - E_{Exs0,\,Grs0}\right) = \frac{\Gamma_{hom}/\pi}{\left(E_{Exs\_p,\,Grs\_p} - E_{Exs0,\,Grs0}\right)^2 + \left(\Gamma_{hom}\right)^2}, \quad (22)$$

The photon density in Exs and Grs is expressed as:

$$\frac{dS_{Exsp}}{dt} = \Gamma v_g \sum_x g_{pxExs} S_{Exsp} - \frac{S_{Exsp}}{\tau_p} + \beta \sum_x \left(L_{Exs}\left(E_{Exs_p} - E_{Exs_x}\right)\frac{N_{Exs}}{\tau_{Exs-r}}\right)\Delta E_p, \quad (23)$$

$$\frac{dS_{Grsp}}{dt} = \Gamma v_g \sum_p g_{pxGrs} S_{Grsp} - \frac{S_{Grsp}}{\tau_p} + \beta \sum_x \left(L_{Grs}\left(E_{Grs\_p} - E_{Grs\_x}\right)\frac{N_{Grs}}{\tau_{Grs-r}}\right)\Delta E_p, \quad (24)$$

where β is the spontaneous coupling factor. *opt* in Equation (13) is the photon density due to the applied EOGB to Exs in a round-trip time τ_{RT} = 2 L/v_g. This term is equal to the number of photons per second per volume irradiating the Exs level in a single round-trip.

$$opt = \frac{P_i\left(2L/v_g\right)}{qE_{Exs\_x}V}, \quad (25)$$

P_i indicates the applied peak power of the Gaussian pulse to Exs.

The parameters used in the simulations are given in Table 1. The values of these parameters were obtained from [13,18–20].

In the algorithm, firstly the constant values and parameters of the laser are determined from Table 1. After that, since the process repeats for every Q-Dot and every mode, the number of modes (i.e., *p*) and number of Q-Dots (i.e., *x*) are defined. As a result, the created simulation consists of three intertwined loops. Before starting all loops, the current is applied to the Wly of the laser. The outermost loop returns as many as the number of quantum dots we have determined (here, our results are relevant to three Q-Dots). In this loop, the energy differences are found with Equation (1). Inside the quantum dot loop, there is a second loop that is repeated according to the mode number. Within the mode loop, the energy differences between the modes are calculated by Equation (2). After these steps are completed, the homogeneous and inhomogeneous broadenings are calculated using Equations (8) and (19). By using the calculated homogeneous and inhomogeneous broadenings and the equations that are numbered as Equations (17), (18) and (20), the material gain and gain compression factor of Exs and Grs are calculated. After that, the third loop that provides the calculation of carrier and photon densities of Exs and Grs is started. In this loop, the rate equations defined as Equations (12)–(14), (23) and (24) are solved using fourth order Runge–Kutta Method. When this loop is completed, the photon and carrier density values of the relevant mode of the related quantum dot is reached. Then, the loops repeated by the number of modes and repeated by the number of quantum dots are finished, respectively. In our study, three Q-Dots and three modes were examined and,

according to this algorithm, there are three modes for each Q-Dot. Since there are three Q-Dots, the center Q-Dot corresponds to the second Q-Dot. Similar to other Q-Dots, there are three modes for the second Q-Dot. Additionally, the results are written using the modes of the center Q-Dot (it is the second Q-Dot for our simulation). The sum of the modes can be calculated by summing the three modes taken from the second Q-Dot.

Table 1. Q-Dot laser parameters.

Cavity length, L 0.245 cm
Cavity width, w 12 μm
Confinement factor, Γ 0.025
Quantum dot density, No 6×10^{16} cm^{-3}
Refractive index, nr 3.27
Cavity internal loss, αint 6 cm^{-1}
Mirror reflectivity, R1, R2 0.95, 0.05
Spontaneous emission ofWly, τwr 500ps
Spontaneous emission of Exs, τer 500ps
Spontaneous emission of Grs, τp 1.2ns
Photon lifetime, τr 8.92 ps
Spontaneous coupling factor, β 1×10^{-4}
Emission energy of Wly, Ewly 1.05 eV
Emission energy of Exs, Eexs 0.840 eV
Emission energy of GS, Egrs 0.792 eV
Phonon relaxation of Wly, Awly 1.35×10^{10} s^{-1}
Auger coefficient of Wly, Cwly 5×10^{-9} cm^3s^{-1}
Phonon relaxation of Wly, Aexs 1.5×10^{10} s^{-1}
Auger coefficient of Exs, Cexs 9×10^{-8} cm^3s^{-1}
Degeneracy of Grs, Exs, Wly, μgrs, exs, wly 2,4,10
Operating frequency, f 1 GHz
Wavelength, λ 1.55 μm
Homogeneous broadening, Γhom 15 meV
Inhomogeneous broadening, Γihom 45 meV

3. Discussion and Results

A 1.55 μm InAs-InP (113)B Q-Dot laser was used in the simulation. The following equation was used to calculate the applied AC current I, with frequency f, and amplitude I_{rf} [21,22].:

$$I(t) = \frac{I_{rf}}{2}(|\cos(2\Pi ft)| - \cos(2\Pi ft)),$$

Unlike previous studies, here, the nonlinear gain was included in multi-population rate equations.

X and P are taken as X = P = 1 (i.e., it was assumed that there are three Q-Dot ensembles) and an Γ_{hom} of 15 meV and Γ_{ihom} of 45 meV has been used in the following results unless stated otherwise. For these values the gain compression factor, $\varepsilon_{Exsp,\ Grsp}$ is calculated as 7.8×10^{-16} cm^3 for Exs and Grs. To observe the radiation simultaneously from both Exs and Grs, the I_{rf} was taken to be 40 mA in the simulations.

Since Γ_{hom} and Γ_{ihom} affect the threshold current (I_{th}), the differential gain and the gain compression factor [10,12], first without EOGB, and the effect of Γ_{hom} and Γ_{ihom} on these mentioned parameters were investigated. Subsequently, an EOGB was applied to the Exs to observe how the optical beam illumination affects the gain-switching output pulses.

The I_{th} was calculated as 30 mA for Exs and 2 mA for Grs for the linear-gain case ($\varepsilon_{Exs,Grs} = 0$) (see Figure 2a); 21 mA for Exs and 2 mA for Grs for the nonlinear-gain case ($\varepsilon_{Exs,Grs} \neq 0$) were obtained (see Figure 2b). The total threshold current (Grs + Exs) for both cases was calculated as 2 mA. As seen in Figure 2b, deviation from Figure 2a due to $\varepsilon_{Exs,Grs}$ is because of the direct relaxation from the Wly to Grs.

Γ_{ihom} changes between 30 and 80 meV at room temperature [23,24], therefore, we changed it from 30 meV to 80 meV. In this case, Γ_{hom} is taken as to be 15 meV at room

temperature [11]. Similarly, since the range of Γ_{hom} is between 10 and 30 meV [2], Γ_{hom} is changed from 10 to 30 meV and Γ_{ihom} is taken to be 45 meV.

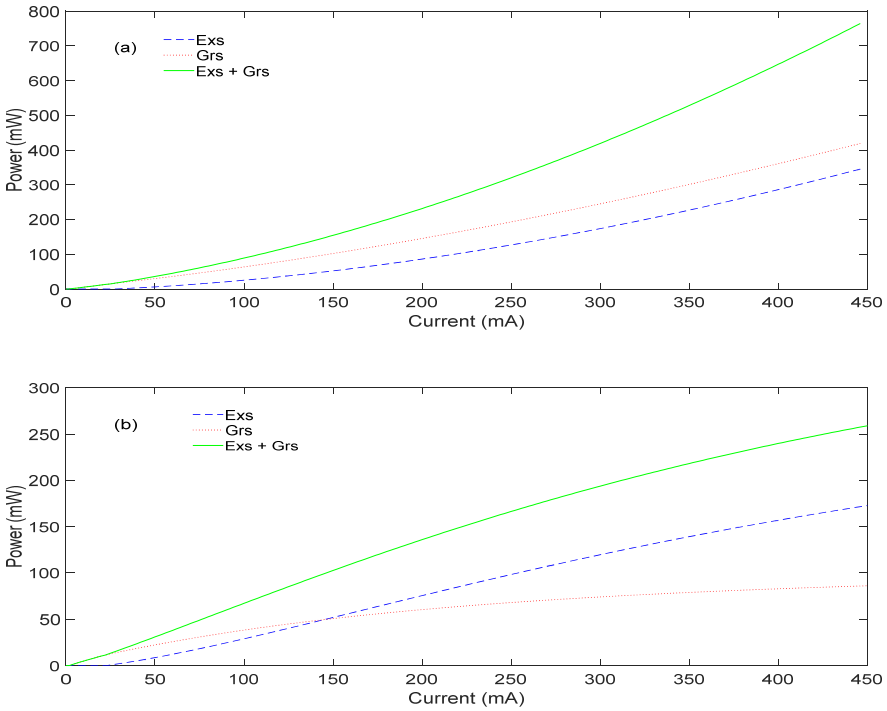

Figure 2. Output power vs. dc current without applying EOGB to the Exs, (**a**) $\varepsilon_{Exs,Grs} = 0$ (**b**) $\varepsilon_{Exs,Grs} \neq 0$.

For the center subgroup of the Q-Dot (second subgroup), when Γ_{ihom} is changed from 30 meV to 80 meV, as the I_{th} of Exs drops from 27 mA to 10 mA the I_{th} of Grs increases from 1 mA to 6 mA (see Figure 3). If Γ_{ihom} is greater than 70 meV, the threshold current increases as the photon density of Grs decreases and finally the threshold currents of Grs and Exs become the same at 11 mA. The effect of Γ_{ihom} on the differential gain is shown in Figure 4. As seen in the figure, as Γ_{ihom} increases, the differential gain of Exs and Grs decreases. Similar results were also observed in [12].

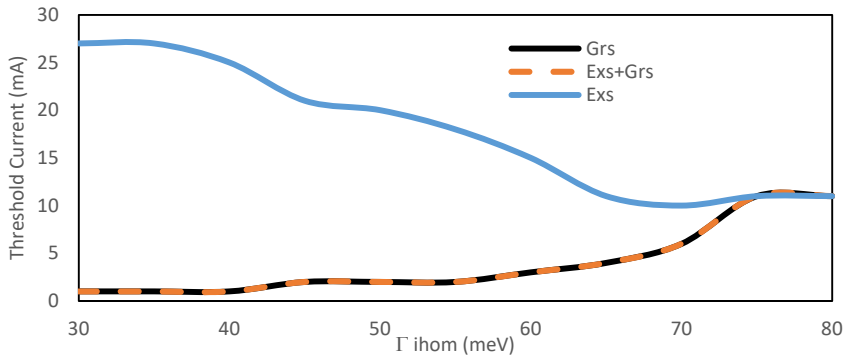

Figure 3. Variation of the threshold current as a function of Γ_{ihom}.

The behavior of Γ_{hom} on I_{th} and on differential gain is similar to that of Γ_{ihom}, providing similar differential gain characteristics as in Figure 4 when Γ_{hom} is increased from 10 meV to 30 meV. For the center subgroup of the Q-Dot, as Γ_{hom} is increased from 10 meV to 30 meV, I_{th} of Exs decreases up to 22.5 meV (dropping from 26 mA to 10 mA) and after that point it slightly increases. I_{th} of Grs increases from 1 mA to 6 mA (see Figure 5). When Γ_{hom} is greater than 22.5 meV the photon density of Grs decreases, whereas the threshold

current increases, yielding a threshold current of 14 mA, which is equal to that of the Exs. Figure 6 indicates the effect of Γ_{hom} on the gain compression factors of Exs and Grs. As seen in the figure, the gain compression factor decreases with the increasing Γ_{hom}.

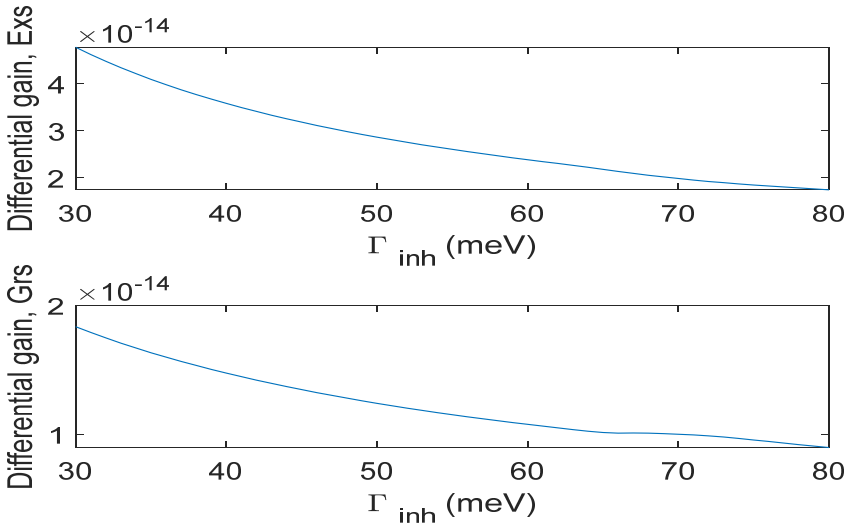

Figure 4. Variation of differential gain as a function of the Γ_{ihom} for I_{rf} = 40 mA.

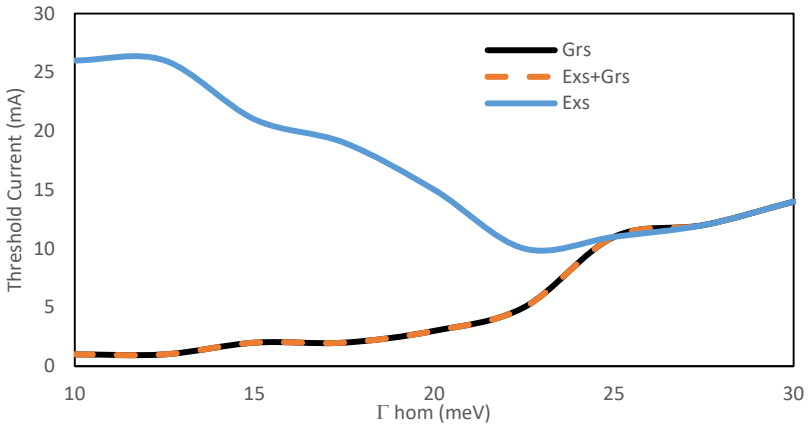

Figure 5. Variation of the threshold current as a function of Γ_{hom}.

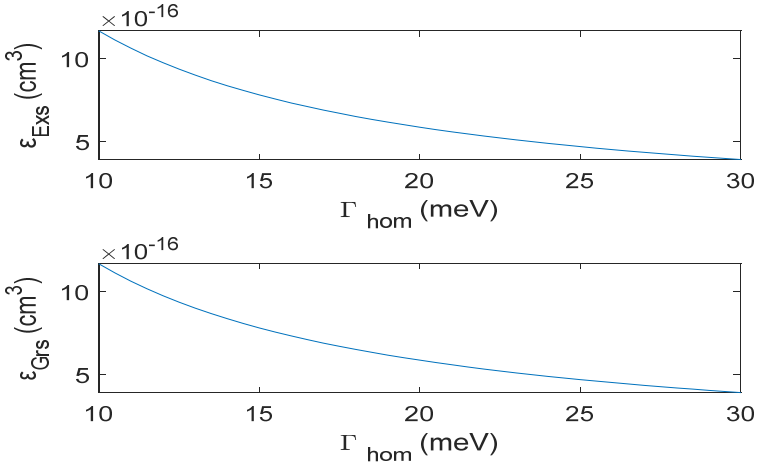

Figure 6. Variation of gain compression factor as function of the Γ_{hom} for I_{rf} = 40 mA.

As seen in the results, the differential gain of Exs is greater than that of the Grs because degeneracy of the Exs is twice that of the Grs. However, the gain compression factor is the same for Grs and Exs. Our results also showed that the output power decreases with the increasing Γ_{hom} and Γ_{ihom}.

As mentioned before, the threshold current was obtained at 2 mA for the Grs and 24 mA for the Exs for the nonlinear-gain case. Therefore, to observe the gain-switched output pulses and also the simultaneous emission from both the Grs and the Exs, we applied I_{rf} of 40 mA. Figure 7 indicates the gain-switched output pulses for an I_{rf} of 40 mA. As shown in the figures, the Grs pulse width is longer (370 ps), while the Exs pulse width is narrow (43 ps). It can be also observed from the figure that the Exs and Grs together contribute to the output pulses since the applied current magnitude is greater than the threshold currents of both states. Therefore, the generated pulses are due to both Exs and Grs emission. The total (Exs + Grs) pulse width is 255 ps and the peak power is 28 mW. As seen in the results, the pulse width of the gain-switched output pulses are long. We also observed that increasing the injection current leads to both the peak power and pulse width increasing. The reason for the increase in the output pulse width with the current is that, although the photon density of the Grs increases with the current, the Grs photon density decreases slowly after reaching the maximum value, as seen in Figure 7. However, the Exs photon density decreases rapidly compared to that of the Grs, yielding a shorter output pulse. It can be said that the long pulses in the InAs-InP (113)B lasers are emitted from the InP ground state.

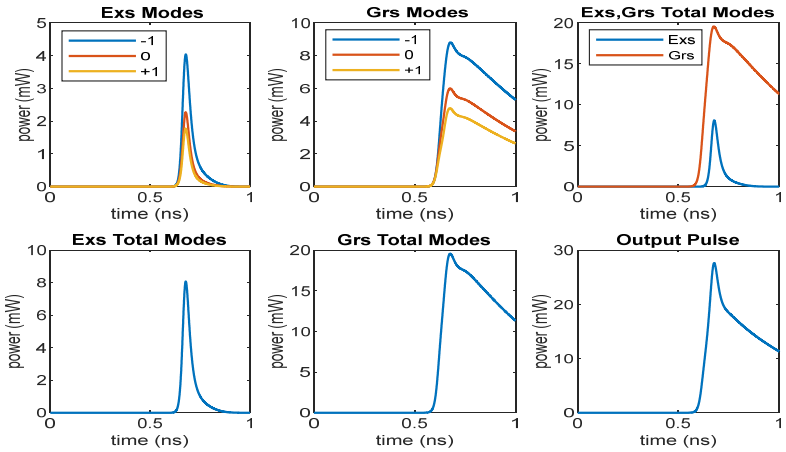

Figure 7. Output pulses for an I_{rf} current of 40 mA.

For InGaAs-GaAs lasers, it was shown that [22] Grs emission is completely saturated in the light-current characteristics, while the Exs emission increases with the increasing current. As a result, if the injection current is increased, the Exs radiation becomes dominant over that of Grs, yielding shorter pulses owing to Exs radiation. Investigation on the InAs-GaAs monolithic Q-Dot lasers revealed that, when the applied injection current increases, the width of the gain-switched pulse decreases [25]. However, in the case of InAs-InP (113)B lasers, the Grs emission does not go to saturation completely (see Figure 2) with the increasing injection current, instead both Grs and Exs emissions increase with the increasing current. Therefore, as mentioned before, the output pulse width of InAs-InP lasers increases with the increasing injection current as compared to that of InAs-GaAs lasers.

Furthermore, our results showed that as Γ_{hom} and Γ_{ihom} increase the I_{th} of Exs decreases, whereas I_{th} of Grs increases (see Figures 3 and 5). Therefore, according to the magnitude of the applied current, even with a smaller value of Γ_{ihom}, the contribution of Exs to output pulses is possible. In order to show this, 25 mA of I_{rf} current is applied and the gain-switched output pulses were obtained for Γ_{ihom} = 30 meV ($\Gamma_{ihom} < \Delta E_{dif} = E_{Exs0}$-$E_{Grs0}$ =48 meV) and Γ_{ihom} = 55 meV ($\Gamma_{ihom} > \Delta E_{dif}$ = 48 meV). As seen in Figures 8 and 9, the output pulse with a full-width half-maximum (FWHM) of 386 ps and peak power

of 26 mW for Γ_{ihom} = 30 meV is generated from Grs emission only. However, since I_{th} of Exs decreased for Γ_{ihom} = 55 meV, both Grs and Exs contribute the output pulse providing an FWHM of 233 ps and peak power of 10 mW. If we apply a current greater than the peak current of 25 mA, for example 60 mA for Γ_{ihom} = 30 meV, both Grs and Exs contribute to the lasing process simultaneously, as shown in Figure 10 producing an FWHM of 478 ps and peak power of 53 mW. Briefly, we can say that the contribution of Exs to gain-switched output pulses depend on not only the value of Γ_{ihom}, which is smaller or greater than the energy difference between Exs and Grs, but also on the magnitude of the applied current. In addition, it can be also observed from the results that the width of pulses are long due to dominant effect of the Grs emission as mentioned before. Wang et al. [12] showed that if Γ_{ihom} is smaller than the energy difference between Exs and Grs (ΔE_{dif} = E_{Exs0}-E_{Grs0}), lasing occurs only due to Grs if Γ_{ihom} is greater than the ΔE_{dif}; both Grs and Exs contribute to the lasing process. However, as seen from our results, Exs lasing depends on the magnitude of current as well as on the value of Γ_{ihom}.

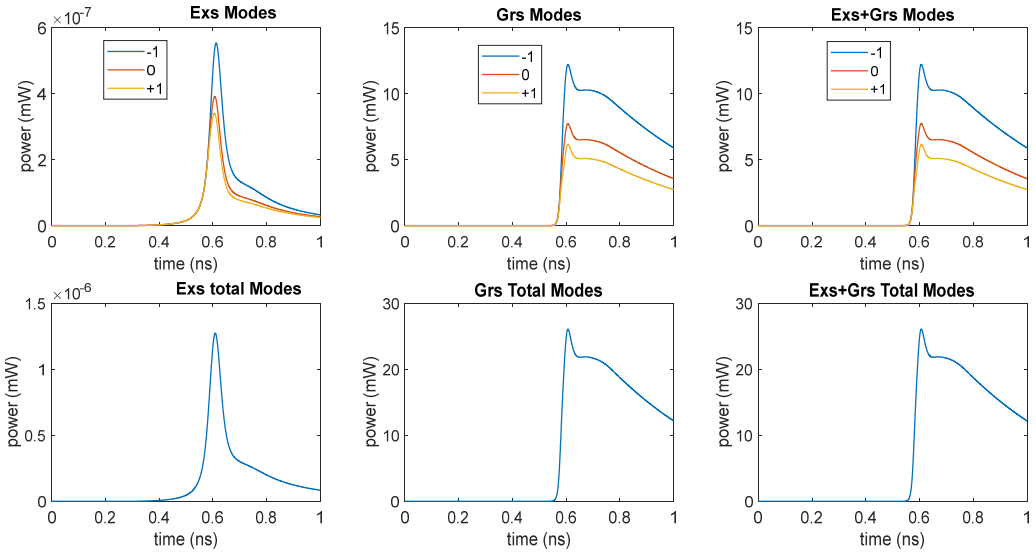

Figure 8. Output pulses for an I_{rf} current of 25 mA for Γ_{ihom} = 30 meV.

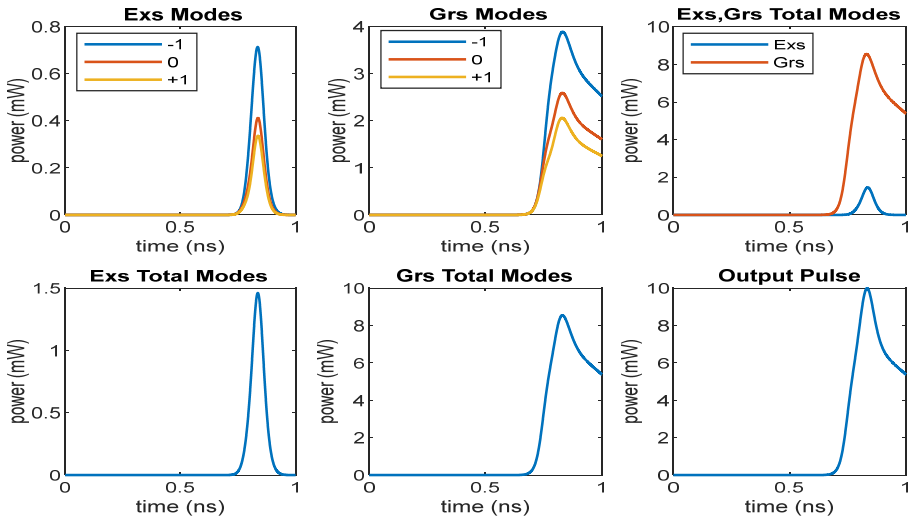

Figure 9. Output pulses for an I_{rf} current of 25 mA for Γ_{ihom} = 55 meV.

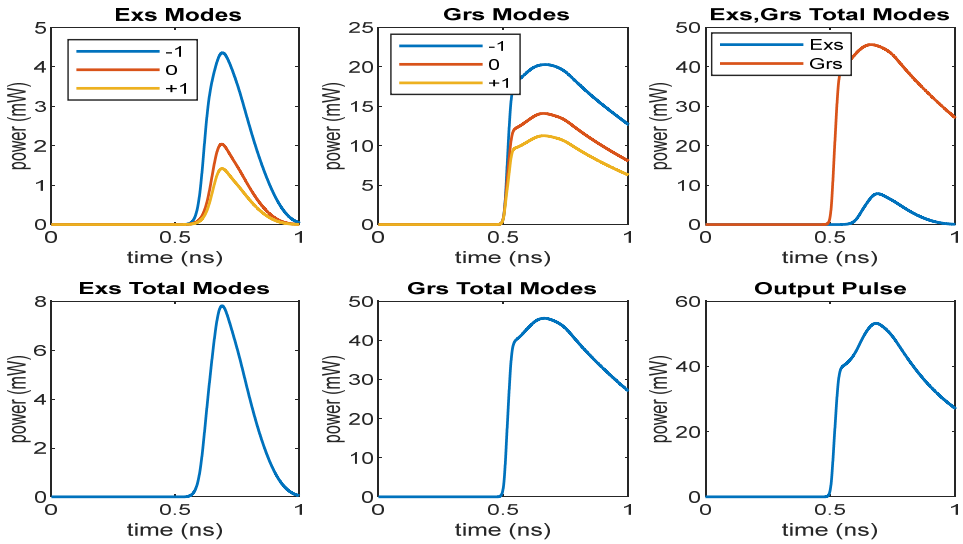

Figure 10. Output pulses for an I_{rf} current of 60 mA for Γ_{ihom} = 30 meV.

According to obtained results, we can say that it is impossible to generate gain-switched short pulses with a high peak power as long as the Grs emission is dominant over the Exs emission for InAs-InP QD lasers. Since the threshold current of Exs is much higher than that of Grs and increasing the injection current makes both Grs and Exs emissions increase, Exs emissions cannot be dominant over Grs emissions. Therefore, in order to obtain gain-switched short pulses with high peak power at low currents, the Exs emission must be sustained while Grs emission must be suppressed. For this reason, an external Gaussian pulse beam to the Exs was applied. When an optical beam is applied to the Exs, depending on the peak value of the applied optical beam, the threshold currents of Grs and Exs can become zero (see Figure 11). Furthermore, the photon density of the Exs can exceed that of the Grs up to a certain current range. This yields gain-switched short pulses exhibiting high power at low currents. Figure 11 shows light vs. dc current characteristics obtained by applying an EOGB with a peak power of 10 mW and a width of 10 ps. In order to see the zero-threshold current for both the states, the dc current was applied up to 50 mA. As seen in the figure, the power of Exs is greater than that of the Grs up to some current value with the application of optical beam and the threshold currents become zero for both states as explained before.

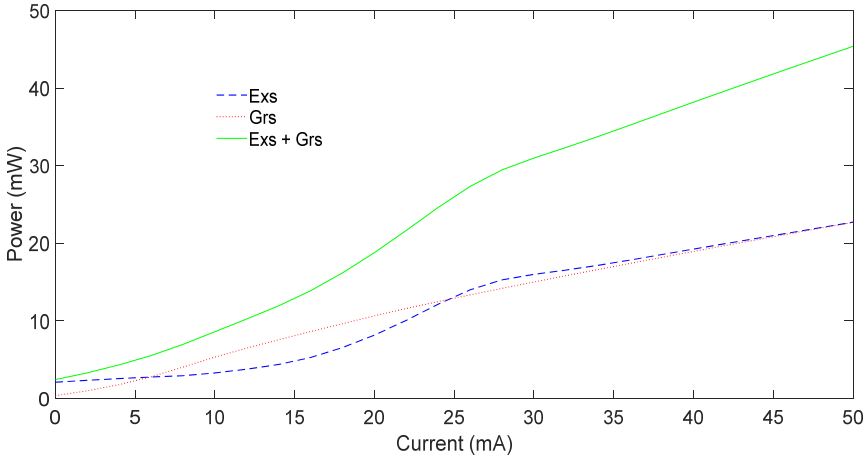

Figure 11. Output power vs. dc current under the EOGB illumination of 10 mW.

Figure 12 indicates the gain-switched output pulses under the optical beam having a peak power of 10 mW and a width of 10 ps for I_{rf} of 12 mA. As seen in the figure, Exs

emission is dominant over Grs emission, which means the output pulse is generated due to Exs emission. Therefore, the width of the output pulse is narrow (26 ps) and the peak power is high (82 mW) even though the applied current is low. Additionally, the peak power of EOGB must be increased to further increase the peak power of the output pulse. Figure 13 shows output pulses for an optical beam peak power of 20 mW for I_{rf} of 12 mA. As seen in the figure, while the peak power of the output increases, the width of the output pulse slightly increases and provides a value of 27 ps. Furthermore, according to the applied current, we can adjust the magnitude of the optical beam to obtain short pulses.

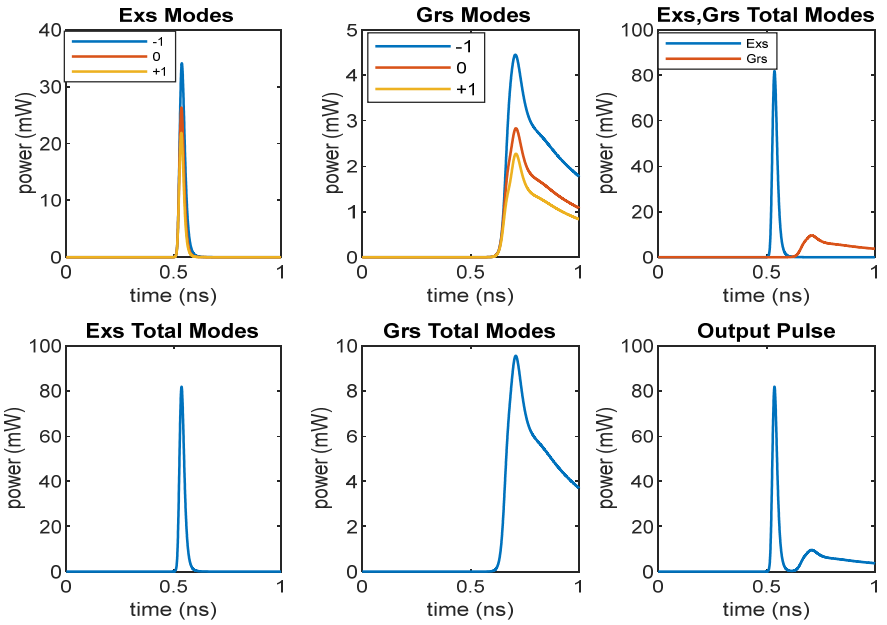

Figure 12. Output pulse under the illumination of an EOGB of 10 mW for I_{rf} = 12 mA.

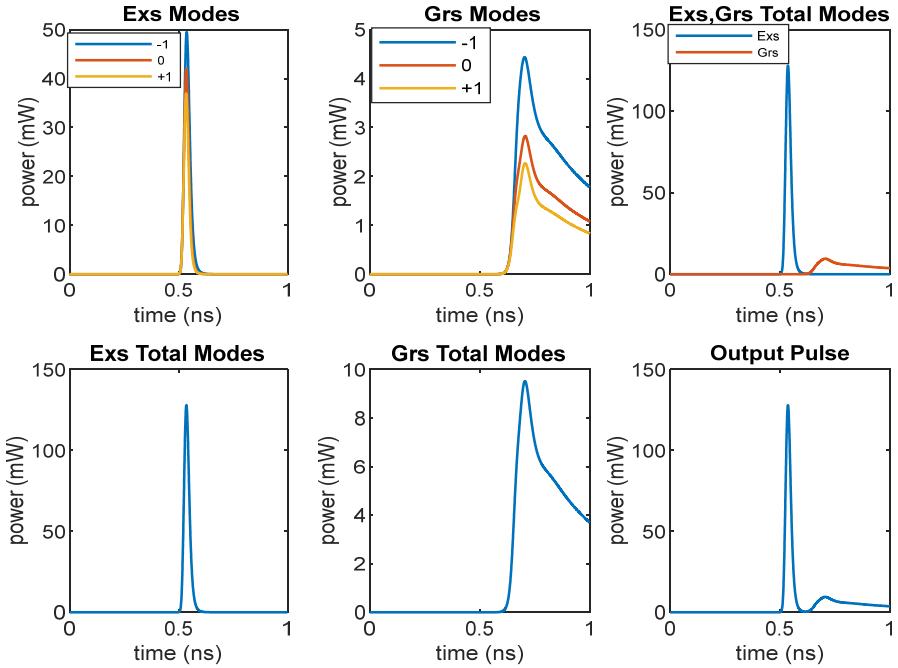

Figure 13. Output pulse under the illumination of an EOGB of 20 mW for I_{rf} = 12 mA.

It was also found that changes in the laser parameters do not affect the output pulse width and peak power significantly in the presence of the optical beam. However, without

EOGB, the output pulses are strongly affected by the change in the laser parameters. Similar results were also obtained for the InAs-InP (113)B quantum dot laser based on single mode rate equations [26].

Regarding the zero-gain compression factor, our results demonstrated that the behavior of gain-switching characteristics with and without EOGB are similar for liner-gain and nonlinear-gain cases except that higher peak power and narrower output pulses are obtained for the linear-gain case.

As a conclusion, when an EOGB is applied to the Exs, the photon emission of Exs becomes dominant over the Grs, providing shorter output pulses with a high peak power. The Exs emission can be tuned for the C-band optical communication window with proper band energy engineering and growth optimization, such as the double cap procedure [27,28].

4. Conclusions

In this study, for the first time, the gain-switching properties have been theoretically investigated in detail in the absence and presence of optical beam illumination for direct the relaxation model of InAs-InP (113)B Q-dot lasers. The model is based on multi-population rate equations involving nonlinear gain. The first effect of the homogeneous and the inhomogeneous broadenings on the differential gain, the gain compression factor, and the threshold current was examined in the absence of the optical beam. Subsequently, the gain-switched output pulses were studied in the absence and presence of optical beam illumination. Our results indicated the following:

(1) The differential gain and the gain compression factor decrease with the increasing homogeneous and inhomogeneous broadenings. However, while the threshold current of the ground state increases, that of the excited state decreases as the broadenings are increased.
(2) While gain-switched pulses are produced only due to ground state emission at small currents, the Exs and Grs emissions contribute to the output pulses at greater currents values (greater than the threshold currents of both excited state and ground state). Since the photon density of the ground state decreases gradually after reaching its maximum value, the output pulses originating from ground state emission have long pulse widths. On the other hand, the photon density of the excited state decreases rapidly after reaching its maximum value, yielding a narrower pulse width. Therefore, when an optical Gaussian pulse beam is applied to the quantum dot laser, gain-switching shorter pulses with high peak power are obtained since excite state emissions dominate ground state emissions.
(3) The contribution of excited state to gain-switched output pulses depend on the magnitude of the applied current as well as on the value of the inhomogeneous broadening.
(4) In the absence of the optical beam, the laser output is strongly affected by the change in the laser parameters, whereas in the presence of the optical beam, this effect is negligible.
(5) The behavior of gain-switching characteristics with and without a Gaussian pulse beam are similar for liner-gain and nonlinear-gain cases except that higher peak power and narrower output pulses are obtained for the linear-gain case.

As a result, short pulses with a width of around 26 ps with a high peak power can be generated at low currents by applying an external optical beam to the Exs. These results showed that InAs-InP (113)B quantum dot lasers are a candidate source for many applications as well as optical communication systems.

A more sophisticated model such as the investigation of the electron-hole model for multi-population rate equations would be the subject of future work.

Author Contributions: Methodology, N.D.; software, H.S.D.T. and E.C.; investigation, N.D., H.S.D.T. and E.C.; writing—original draft preparation, N.D.; supervision, N.D.; project administration, N.D. All authors have read and agreed to the published version of the manuscript.

Funding: This research was funded by The Scientific and Technological Research Council of Turkey (TUBITAK), grant number 119F099.

Data Availability Statement: Not applicable.

Conflicts of Interest: The authors declare no conflict of interest.

References

1. Shimizu, M.; Suzuki, Y.; Watanabe, M. Characteristics of Cavity Round-Trip Time Pulses in Short-Cavity Q-Switched AlGaAs Multiple-Quantum-Well Semiconductor Lasers. *Jpn. J. Appl. Phys.* **1998**, *37*, 1040. [CrossRef]
2. Grillot, F.; Veselinov, K.; Gioannini, M.; Montrosset, I.; Even, J.; Piron, R.; Homeyer, E.; Louaiche, S. Spectral Analysis of 1.55-m InAs–InP(113)B Quantum-Dot Lasers Based on a Multipopulation Rate Equations Mode. *IEEE J. Quantum Electron.* **2009**, *45*, 872. [CrossRef]
3. Caroff, P.; Paranthoen, C.; Platz, C.; Dehaese, O.; Folliot, H.; Bertru, N.; Labbe, C.; Piron, R.; Homeyer, E.; Le Corre, A.; et al. High gain and low-threshold InAs QD lasers on InP. *J. Appl. Phys.* **2005**, *87*, 243107.
4. Saito, H.; Nishi, K.; Kamei, A.; Sugou, S. Low chirp observed in directly modulated quantum dot lasers. *IEEE Photon. Technol. Lett.* **2000**, *12*, 1298. [CrossRef]
5. Reithmaier, J.P.; Forchel, A. Recent advances in semiconductor quantum-dot lasers. *C. R. Phys.* **2003**, *4*, 611. [CrossRef]
6. Huang, H.; Duan, J.; Jung, D.; Liu, A.Y.; Zhang, Z.; Norman, J.; Bowers, J.E.; Frédéric, G. Analysis of the optical feedback dynamics in InAs/GaAs quantum dot lasers directly grown on silicon. *J. Opt. Soc. Am. B* **2018**, *35*, 2780. [CrossRef]
7. Rafailov, E.U.; Cataluna, M.A.; Sibbett, W. Mode-locked quantum-dot lasers. *Nat. Photonics* **2007**, *1*, 395–401. [CrossRef]
8. Sritirawisarn, N.; Otten FW, M.; van Eijkemans, T.J.; Nötzelet, R. Surface morphology induced InAs quantum dot or dash formation on InGaAs/InP(100). *J. Cryst. Growth* **2007**, *305*, 63. [CrossRef]
9. Heck, S.C.; Osborne, S.; Healy, S.B.; O'Reilly, E.P.; Lealarge, F.; Pointgt, F.; Le Gouezigou, O.; Accard, A. Experimental and theoretical study of InAs/InGaAs/InP quantum dash laser. *IEEE J. Quantum Electron.* **2009**, *45*, 1508. [CrossRef]
10. Sugawara, M.; Mukai, K.; Nakata, Y.; Ishikawa, H. Effect of homogeneous broadening of optical gain on lasing spectra in self-assemled $In_xGa_{1-x}As$/GaAs quantum dot lasers. *Phys. Rev.* **2000**, *61*, 7595. [CrossRef]
11. Grillot, F.; Veselinov, K.; Gioannini, M.; Piron, R.; Homeyer, E.; Even, J.; Loualiche, S.; Montrosset, I. Theoretical analysis of 1.55-µm InAs/InP (113)B quantum dot lasers based on a multi-population rate equation model. In Proceedings of the Physics and Simulation of Optoelectronic Devices XVII, San Jose, CA, USA, 24 February 2009; Volume 7211.
12. Wang, C.; Gionnini, M.; Montrosset, I.; Even, J.; Grillot, F. Influence of inhomogeneous broadening on the dynamics of quantum dot lasers. In Proceedings of the SPIE OPTO, Physics and Simulation of Optoelectronic Devices XXIII, San Francisco, CA, USA, 28 April 2015; Volume 9357.
13. Aleem, M.N.A.; Huessein, K.F.A.; Ammar, A.A. Semiconductor quantum dot lasers as pulse sources for high bit rate data transmission. *PIER* **2013**, *28*, 185. [CrossRef]
14. Gioannini, M.; Rossetti, M. Time-domain traveling wave model of quamtum dot DFB lasers. *IEEE J. Sel. Top. Quantum Electron.* **2011**, *17*, 1318. [CrossRef]
15. Gioannini, M.; Bardella, P.; Montrosset, I. Time-domain traveling-wave analysis of multimode dynamics of quantum dot Fabry-Perot lasers. *IEEE J. Sel. Top. Quantum Electron.* **2015**, *21*, 1900811. [CrossRef]
16. Veselinov, K.; Grillot, F.; Miska, P.; Homeyer, E.; Caroff, P.; Platz, C.; Even, J.; Dehaese, O.; Loualiche, S.; Marie, X.; et al. Carrier dynamics and saturation effects in (311)B InAs-InP quantum dot lasers. *Opt. Quantum Electron.* **2006**, *38*, 369. [CrossRef]
17. Xu, D.V.; Yoon, S.F.; Tong, C.Z. Self-consistent analysis of carrier confinement and output power in 1.3-µm InAs-GaAs quantum dot VCSELs. *IEEE J. Quantum Electron.* **2008**, *44*, 879. [CrossRef]
18. Dogru, N.; Adams, M.J. Intensity noise of actively mode-locked quantum dot external cavity laser. *J. Light. Technol.* **2014**, *32*, 3215. [CrossRef]
19. Dogru, N.; Adams, M.J. Numerical simulation of a mode-locked quantum dot external cavity laser. *IET Optoelectron.* **2014**, *8*, 44. [CrossRef]
20. Veselinov, K.; Grillot, F.; Cornet, C.; Even, J.; Bekaiarski, A.; Gioannini, M.; Loualiche, S. Analysis of the double laser emission occurring in 1.55-µm InAs-InP(113)B quantum-dot lasers. *IEEE J. Quantum Electron.* **2007**, *43*, 810. [CrossRef]
21. Avrutin, E.; Ryvkin, B.; Kostamovaara, J.; Kuksenkov, D. Strongly asymmetric waveguide laser diodes for high brightness picosecond optical pulses generation by gain switching at GHz repetition rates. *Semicond. Sci. Technol.* **2015**, *30*, 055006. [CrossRef]
22. Avrutin, E.A.; Dogru, N.; Ryvkin, B.; Kostamovaara, J.T. Spectral control of asymmetric-waveguide large signal modulated diode lasers for non-linear applications. *IET Optoelectron.* **2016**, *10*, 57. [CrossRef]
23. Bhattacharya, P.; Klotzkin, D.; Qasaimeh, O.; Zhou, W.; Krishna, S.; Zhu, D. High-speed modulation and switching characteristics of In(Ga)As-Al(Ga)As self-organized quantum-dot lasers. *IEEE J. Sel. Top. Quantum Electron.* **2000**, *6*, 426. [CrossRef]

24. Cornet, C.; Labbe, C.; Folliot, H.; Bertru, N.; Dehaese, O.; Even, J.; Le Corre, A.; Paranthoen, C.; Platz, C.; Loualiche, S. Quantitative investigation of optical absorption in InAs/InP (311)B quantum dots emitting at 1.55 μm wavelength. *Appl. Phys. Lett.* **2004**, *85*, 5685. [CrossRef]
25. Hantschmann, C.; Vasil'ev, P.P.; Chen, S.; Liao, M.; Seeds, A.J.; Liu, H.; Penty, R.V.; White, I.H. Gain switching of monolithic 1.3 μm InAs/GaAs quantum dot lasers on silicon. *J. Light. Technol.* **2018**, *36*, 3837. [CrossRef]
26. Dogru, N.; Duranoglu Tunc, H.S.; Al-Dabbagh, A.M. Gain-switched short pulse generation from InAs-InP(113)B quantum dot laser excited state. *Opt. Laser Technol.* **2022**, *148*, 107709. [CrossRef]
27. Paranthoen, C.; Bertru, N.; Dehaese, O.; Loualiche, S.; Lmabert, B. Height dispersion control of InAs/InP(113)B quantum dots emitting at 1.55 μm. *Appl. Phys. Lett.* **2001**, *78*, 1751. [CrossRef]
28. Koenraad, P.M.; Bertru, N.; Bimberg, D.; Loualiche, S. Electronic and optical properties of InAs/InP quantumdots on InP(100) and InP(311)B substrates: Theory and experiment. *Phys. Rev. B* **2006**, *74*, 035312.